Engineered Regeneration 5 (2024) 80–91

Contents lists available at ScienceDirect

Engineered Regeneration

journal homepage: http://www.keaipublishing.com/en/journals/engineered-regeneration/

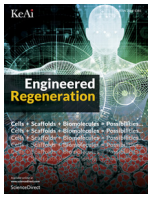

Pulsed electromagnetic field stimulation enhances neurite outgrowth in neural cells and modulates inflammation in macrophages

Francesco Fontana[a,b,*], Andrea Cafarelli[a,b], Francesco Iacoponi[a,b], Soria Gasparini[a,b], Tiziano Pratellesi[c], Abigail N. Koppes[d,e,f], Leonardo Ricotti[a,b]

[a] The BioRobotics Institute, Scuola Superiore Sant'Anna, 56127 Pisa, Italy
[b] Department of Excellence in Robotics & AI, Scuola Superiore Sant'Anna, 56127 Pisa, Italy
[c] BAC Technology s.r.l., 50063 Florence, Italy
[d] Department of Chemical Engineering, Northeastern University, Boston, MA 02115, USA
[e] Department of Bioengineering, Northeastern University, Boston, MA 02115, USA
[f] Department of Biology, Northeastern University, Boston, MA 02115, USA

ARTICLE INFO

Keywords:
Nerve regeneration
Biophysical stimulation
Pulsed electromagnetic fields (PEMF)
Neurite outgrowth
Anti-inflammatory
Peripheral nerve injuries

ABSTRACT

Nerve regeneration following traumas remains an unmet challenge. The application of pulsed electromagnetic field (PEMF) stimulation has gained traction for a minimally invasive regeneration of nerves. However, a systematic exploration of different PEMF parameters influencing neuron function at a cellular level is not available. In this study, we exposed neuroblastoma F11 cells to PEMF to trigger beneficial effects on neurite outgrowth. Different carrier frequencies, pulse repetition frequencies, and duty cycles were screened with a custom *ad hoc* setup to find the most influential parameters values. A carrier frequency of 13.5 MHz, a pulse repetition frequency of 20 Hz, and a duty cycle of 10% allowed maximal neurite outgrowth, with unaltered viability with respect to non-stimulated controls. Furthermore, in a longer-term analysis, such optimal conditions were also able to increase the gene expression of neuronal expression markers NeuN and Tuj-1 and transcription factor Ngn1. Finally, the same optimal stimulation conditions were also applied to THP-1 macrophages, and both pro-inflammatory (TNF-α, IL-1β, IL-6, IL-8) and anti-inflammatory cytokines (IL-10, CD206) were analyzed. The optimal PEMF stimulation parameters did not induce differentiation towards an M1 macrophage phenotype, decreased IL-1β and IL-8 gene expression, decreased TNF-α and IL-8 cytokine release in M1-differentiated cells, increased IL-10 and CD206 gene expression, as well as IL-10 cytokine release in M0 cells. The specific PEMF stimulation regime, which is optimal *in vitro,* might have a high potential for a future *in vivo* translation targeting neural regeneration and anti-inflammatory action for treating peripheral nerve injuries.

1. Introduction

Peripheral nerve injuries increased in the last decade [1] representing 2% of all traumas affecting the body's extremities [2]. Following injury, peripheral nerves retain some ability to regenerate, which depends on the patient's age, the injury mechanism, the time to intervention, the injury size, and the distance from the nerve cell body [3].

As regards the currently applicable treatments following peripheral nerve injuries, no definitive solutions have been found yet: physical therapies, for example, often lack efficacy in rehabilitation; pharmacological treatments primarily focus on pain alleviation and can have side effects [4]; surgery-based strategies are hardly and invasively implemented, and can induce immunosuppression [5]; tissue engineering solutions comprise of nerve conduit implants, which can also be difficult to perform and hardly reproduce the extracellular matrix. Therefore, clinical results after large nerve gap repair are often not satisfactory and with seldom recovered functionality, so motivating the search for different approaches.

It is known that peripheral nerve injury also triggers a robust neuroinflammatory response [6], mainly due to the action of macrophages: they are in fact recruited to pursue debris elimination and tissue remodeling [7] through complex signaling pathways with sensory neurons and Schwann cells, with a central role played by cytokines and chemokines [8]. In particular, pro-inflammatory cytokines (*e.g.,* interleukin (IL)−6 and tumor necrosis factor-alpha (TNF-α)) are secreted mainly in the first phase of the inflammatory response, fostering the recruitment of macrophages 2–3 days after injury. Anti-inflammatory cytokines (*e.g.,* IL-10) are secreted after macrophage recruitment and attenuate the in-

* Corresponding author at: The BioRobotics Institute, Scuola Superiore Sant'Anna, 56127 Pisa, Italy.
E-mail address: francesco.fontana16@unibo.it (F. Fontana).

https://doi.org/10.1016/j.engreg.2023.11.003
Received 26 May 2023; Received in revised form 28 November 2023; Accepted 30 November 2023
Available online 16 December 2023

flammatory process. Promoting the endogenous anti-inflammatory reaction and reducing pro-inflammatory processes might lead to develop new therapeutic protocols able to accelerate and improve peripheral nerve regeneration.

In this challenging scenario, electromagnetic fields, sometimes combined with growth and trophic factors, represent an exciting approach for nerve repair thanks to several advantages, especially safety, non-invasiveness and low cost [9]. When the electromagnetic wave is transmitted in a pulsed way, the mode is defined as pulsed electromagnetic fields (PEMF), and represents a subset of the extremely low-frequency electromagnetic fields, with a pulsed repetition frequency (PRF) from 5 to 300 Hz [10]. This stimulation regime was demonstrated to have beneficial effects for wound healing, pain treatment, bone formation, and other applications [11–13], so that in 1979 the United States Food and Drug Administration started approving several PEMF devices for the treatment of delayed union or non-union fractures [10]. Nonetheless, until today, the widespread adoption of PEMF in mainstream medicine remains limited and is generally restricted to use by prescription as the underlying biological mechanisms have not been fully understood yet [14].

When considering neuronal cells exposed to PEMF, several studies have been carried out *in vitro*. Zhang et al. [15], for example, stimulated PC12 cells with PEMF (PRF = 1–100 Hz; duty cycle (DC) = 10%; intensity (I) = 0.016, 0.19, 1.37 mT). Differently from the majority of works in the state-of-the-art [16,17,12], the authors screened different stimulation parameters (limited to PRF and I). They identified the most effective values promoting neurite outgrowth. They found that exposure to a relatively high flux density (1.37 mT) and a medium flux density (0.19 mT) inhibited the percentage of neurite-bearing cells and significantly increased neurite length. They also studied the effect of PRF at the constant flux density of 1.37 mT, verifying that a PRF of 50 and 75 Hz benefits neurite outgrowth. A similar approach was followed by Li et al. [18], who varied PEMF I on primary cultures of dorsal root ganglion neurons (PRF = 50 Hz; I = 0.1, 1, 10, 100 mT; t = 2 h), observing an increase in brain-derived neurotrophic factor expression, especially in correspondence of an I = 1 mT.

Regarding macrophages exposed to PEMF, several studies have also been carried out *in vitro*. Ross et al. [19], for example, applied PEMF on lipopolysaccharide (LPS)-treated RAW 264.7 cells, an inflammation model, at the following stimulation conditions: PRF = 5–30 Hz; DC = 50%; I = 4 mT; t = 1 h The authors found that cells exposed to PEMF at 5 Hz showed a considerable downregulation of TNF-α. Groiss et al. [20] stimulated LPS-treated THP-1 cells with PEMF (PRF = 16.7 Hz; I = 0.05, 0.250, and 4.8 mT; t = 10 min on/10 min off for 24 h). The authors observed that the highest flux density significantly increased the gene expression of the anti-inflammatory marker IL-10.

Despite these exciting hints, many aspects still need to be clarified. Indeed, the lack of a systematic screening of different stimulation parameters has already been highlighted as one of the reasons for the poor repeatability of the beneficial effects of PEMF [21]. Besides that, the molecular mechanisms underlying the PEMF-induced effects on neurite outgrowth have not been elucidated yet [22].

In this work, we chose F11 cells as they are an established model for mimicking peripheral injured neurons [23,24]. In particular, being derived from embryonic or neonatal rat dorsal root ganglia neurons by fusion with the mouse neuroblastoma cell line N18Tg2, they exhibit traits of peripheral sensory neurons, such as excitable membranes and sensory neuronal cell surface markers that have been demonstrated to actively react to electromagnetic stimulation [25,26]. Furthermore, this cell line has already been used to study neuronal plasticity and gene regulation during peripheral nervous system regeneration [27,28]. We first characterized the magnetic and electric fields a custom PEMF device produced. Then we applied PEMF stimulation to F11 cells assessing the corresponding effects on cell viability and neurite outgrowth. Three different stimulation parameters (F, PRF and DC) were controlled to identify the most appropriate conditions for triggering regenerative effects in primary neurons.

Then, a longer-term analysis was carried out on F11 cells to verify the effects of the optimal stimulation conditions on the expression of genes featuring neuronal phenotype: NeuN and Tuj-1, as well as the transcription factors Ngn1 and NeuroD. These markers are often used in the state of the art to investigate the activation of neural differentiation [29,30]. This allowed us to explore some molecular mechanisms underlying the PEMF-induced effects on neurite outgrowth. Finally, we applied the optimal stimulation conditions to the human monocytic cell line THP-1, broadly adopted in the state-of-the-art as a representing cell model of part of the inflammatory phenomena occurring in peripheral nerve injury [31,32]. After differentiating cells into M1 and M2 phenotypes by using LPS and IL-4, respectively, the effects of PEMF on cytokine release and gene expression of pro-inflammatory markers (TNF-α, IL-1β, IL-6, IL-8) and anti-inflammatory ones (IL-10 and CD206) were evaluated.

2. Materials and methods

2.1. F11 and THP-1 cell cultures

F11 neural cells (Invitrogen) were seeded onto laminin-coated (50 μg/mL, Thermo-Fisher) coverslips (12 mm radius, Thermo-Fisher) at a density of 20,000 cells/coverslip. Cell density was tested and evaluated to avoid clusters formations that could jeopardize image analyses. The neurons were grown for a total of 72 h in a growth medium (GM) composed of high glucose Dulbecco's Modified Eagle Medium (DMEM, Sigma-Aldrich), supplemented with 1% fetal bovine serum (v/v, FBS, Sigma-Aldrich) and 100 IU/mL penicillin, 100 μg/mL streptomycin (Sigma-Aldrich), under standard conditions (37 °C, 5% CO_2), to foster neurite outgrowth [33]. Seventy-two hours after initial cell plating, the GM was replaced, and cells were subjected to PEMF stimulation for three h/day for three days. Twenty-four hours after the last stimulation, biological analyses were conducted as described below.

THP-1 monocytes (ATCC®) were seeded according to the protocol described by Fontana et al. [34].

2.2. PEMF hardware and stimulation protocols

The PEMF system (Fig. 1) consisted of a wave modulator equipped with four different generators (BAC Technology S.r.l.) that allowed the generation of a signal at four different F; a custom polycarbonate chamber for hosting cells seeded on coverslips (three independent samples);

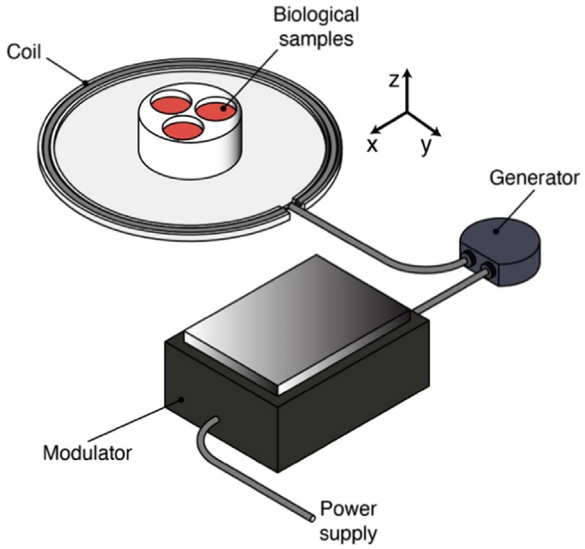

Fig. 1. Depiction of the custom PEMF stimulation system used in this study and its components.

and a circular coil (108 mm diameter, 1 mm single copper wire) surrounding the biological samples.

Considering that previous studies adopted standard PEMF devices that featured only a central F of 27 MHz [35], three additional F values were integrated into our custom device to investigate the influence of this stimulation parameter. Our system allowed setting the F to equal 7.5, 13.5, 27, and 54 MHz. Four quartz of the same type were adopted for each generator to guarantee a ~1% maximum difference when switching F to minimize differences in the transmitted signals. The wave modulator allowed tuning three parameters, so modifying the total amount of energy transmitted to cells: PRF (in the range 1–1000 Hz ± 1 Hz), DC (in the range 1–99% ± 0.5%), and t (1–8 h).

To characterize the field distribution, a measurement of the magnetic and electric fields produced was performed with appropriate probes (100A and 100D, Beehive Electronics) connected to an oscilloscope (7034B, InfiniiVision, Agilent Technologies). The probes were moved in the area within the coil (XY plane – 1 mm step) using a three-axis step-by-step motorized positioning frame (XYZ BiSlide, Velmex, Bloomfield, NY, USA). The probes were placed at a height (z = 5 mm) where biological samples were positioned during the stimulations. Measurements were performed for all the tested F, at a DC of 100%. PEMF output I was set for the system generator and equal to 0.3 mT (correspoding to a magnetic field strength of 240 A/m), and experimentally verified at the coil center (x = 0; y = 0; z = 5 mm) with a calibrated probe (100A and 100D, Beehive Electronics). This I value was frequently adopted in the state-of-the-art [36–39].

Regarding the F11 stimulation protocol, three parameters were consecutively varied in the experiment, one at a time: F, PRF, and DC (t was fixed at 3 h/d, for three days, for all the experiments). F was varied first (testing 7.5, 13.5, 27, and 54 MHz), setting a PRF of 50 Hz and a DC of 10%. Once the optimal F was identified, PRF was varied (considering 5, 20, 50, and 75 Hz), setting the optimal F previously identified and a DC of 10%. Once the optimal PRF was found, DC was varied (10, 20, 30, and 40%), setting the optimal F and the optimal PRF previously identified.

Once the optimal stimulation conditions were found (optimal F, optimal PRF, and optimal DC), these conditions were applied again to F11 cells for a longer-term analysis. Two experimental groups and three time points were identified (the stimulation protocol was the same as previously mentioned). The experimental groups were “Ctrl” and “PEMF” which respectively represented the unstimulated and stimulated samples; the three timepoints were: “d1” corresponding to 24 h after PEMF stimulation; “d3” corresponding to 3 days after PEMF stimulation; and “d10” corresponding to 10 days after PEMF stimulation.

Finally, the optimal PEMF stimulation conditions were applied to THP-1 cells, identifying five experimental groups: *(i)* “M0”, in which M0 macrophages were cultured in GM for three days; *(ii)* “M1”, in which M0 macrophages were treated with LPS and then kept in GM for three days; *(iii)* “M2”, in which M0 macrophages were treated with IL-4 and then kept in GM for three days; *(iv)* “M0+PEMF”, in which M0 macrophages were stimulated with PEMF for three days at the optimal stimulation conditions; *(v)* “M1+PEMF”, in which M0 macrophages were treated with LPS and then stimulated with PEMF for three days at the optimal stimulation conditions.

2.3. Immunostaining on F11 cells

24 h after the last stimulation, F11 cells were fixed in 4% paraformaldehyde (v/v) (PFA, Sigma-Aldrich) for 30 min, permeabilized with 0.1% Triton X-100 (Sigma-Aldrich) for 30 min, and blocked with 2.5% (v/v) Goat Serum (Sigma Aldrich) for 2 h Samples were incubated with a primary antibody Monoclonal Anti-β-Tubulin III (Invitrogen) (1:250), for 1 h at room temperature, in the dark. Samples were washed thrice with 1X Hanks’ Balanced Salt Solution (HBSS, Sigma-Aldrich, 5 min each time). A secondary antibody, Goat anti-Mouse IgG (H + L) Highly Cross-adsorbed, Alexa Fluor™ Plus 555 (Invitrogen) (1:1000) diluted in 2.5% (v/v) goat serum was then added and incubated for 1 h at room temperature, in the dark. Before imaging, samples were washed thrice with 1X HBSS (5 min each). 4′, 6′-damidino-2-phenylindole (DAPI, Invitrogen) (1:500) was added 10 min before imaging. All immunofluorescence images were acquired with an upright fluorescence microscope (Zeiss Axio Observer, Carl Zeiss Microscopy LLC).

2.4. Analysis of immunofluorescence images

All neuron images were analyzed using the Neurolucida tracing software (Neurolucida 11.03, MFB Bioscience) according to established methods [40–42]. The quantification of neuromorphometrics was carried out regarding neural extension mean length. In particular, for each experiment, a “Neurite length” variable was defined as follows: (Dendrites Mean Length * Number of Dendrites) / Number of body cells. The seeding density of neurons was selected to maximize cells within the central part of the coverslip, limiting at the same time the number of neurites that would have contacted adjacent neurons (so creating clusters) or the edge of the coverslip (so, producing contact-dependent effects). The same density was held constant within each experimental condition.

2.5. Assessment of F11 cell viability

AlamarBlue reagent (Invitrogen) was used following the manufacturer’s instructions to analyze PEMF’s impact on neural cell viability. For this procedure, F11 cells were seeded at a density of 20,000 cells/coverslip as previously described and grown for 72 h in standard incubation settings (37 °C, 5% CO_2). Then, the GM was removed and replaced with 1 mL of fresh medium. Following medium replacement, cells were subjected to a stimulation session or left unstimulated as a control, following the previously mentioned stimulation protocols. After the last stimulation, cells were returned to the incubator and grown for an additional 24 h 100 μL of the AlamarBlue reagent was added to each well, gently mixed by swirling, and returned to the incubator for 2 h Following the 2 h incubation time with AlamarBlue, 100 μL of the GM containing the reagent was transferred to a glass-bottom black 96-well plate and analyzed in terms of fluorescence intensity (A.U.) on an EnSight plate reader (PerkinElmer) (excitation wavelength: 550 nm; emission wavelength: 590 nm). By normalizing the A.U. to the control mean value, the fold change in viability for each experimental group was determined.

2.6. Enzyme-linked immunosorbent assay (ELISA) analyses on THP-1 cells

As regards THP-1 cells, the supernatant was collected 24 h after the last stimulation, and IL-1β, IL-6, IL-8, IL-10, and TNF-α cytokine release were analyzed with Human IL-1β ELISA Kit (Invitrogen), Human IL-6 ELISA Kit (Sigma-Aldrich), Human IL-8 ELISA Kit (Invitrogen), Human IL-10 ELISA Kit (Sigma-Aldrich) and Human TNF-α ELISA Kit (Invitrogen), according to the manufacturer’s instructions. A VICTOR Nivo Multilabel plate reader (PerkinElmer) read the absorbance signal, setting a primary wavelength of 450 nm for all the kits.

2.7. Real-time quantitative reverse transcription polymerase chain reaction (qRT-PCR) analyses on F11 and THP-1 cells

The total RNA collection, the reverse transcription and the qRT-PCR were performed following the same procedure described in Fontana et al. [31]. Forward and reverse primers for Real-Time qRT-PCR amplification of NeuN, Tuj-1, Ngn1, NeuroD, IL-1β, IL-6, IL-8, IL-10, TNF-α, and CD206 are listed in Table S1. The relative gene expressions were normalized to GAPDH for F11 cells and 18SrRNA for THP-1 cells, analyzed with the ΔΔC(T) method [40] and expressed as Fold Change with

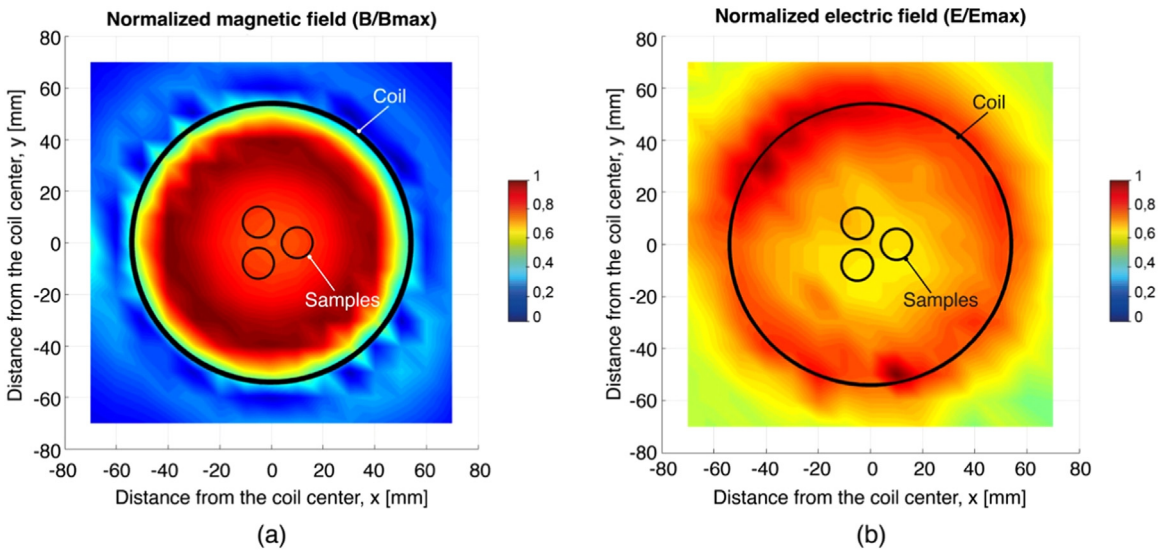

Fig. 2. Measurements of the normalized magnetic (a) and electric (b) field distribution produced by the coil in the PEMF system, for $F = 13.5$ MHz, in the xy plane (step resolution = 1 mm) with $z = 5$ mm. The positions of the coil and biological samples are highlighted with black circles.

respect to the control group ("Ctrl_d1" for F11 cells, "M0" for THP-1 cells).

2.8. Statistical analyses

All data herein presented is derived from at least 3 independent samples for each experiment and each experimental group. GraphPad Prism 9 was used to perform statistical analyses.

Considering the analysis of F11 fluorescence images, at least 5 spots were captured for each biological sample; for each spot, at least 10 neurons were characterized, based on a power analysis previously conducted by Koppes et al. [43]. A Shapiro-Wilk normality test was performed, with a significance threshold of $p = 0.05$, showing a normal distribution. Then, a one-way ANOVA followed by Tukey's post hoc test was applied to identify statistically significant differences between experimental groups ($p = 0.05$).

As regards F11 viability and gene expression tests, as well as analyses performed on THP-1 cells, the Shapiro-Wilk normality ($p = 0.05$) showed a non-normal distribution. Thus, Kruskal-Wallis with Dunn's post-hoc test was applied for identifying statistically significant differences ($p = 0.05$).

For all statistical analyses, statistically signficant differences were represented as follows: $^{*} = p < 0.05$; $^{**} = p < 0.01$; $^{***} = p < 0.001$; $^{****} = p < 0.0001$.

3. Results

3.1. Magnetic and electric field characterization

Measurements of normalized magnetic and electric field distribution are reported in Fig. 2a and b, respectively, for the $F = 13.5$ MHz case. The maps corresponding to the other F values are shown in Fig. S1. The magnetic and electric fields were largely homogeneous in the positions corresponding to the biological samples for all F values. An example of the fast Fourier transform signal acquired at the driving F of 13.5 MHz is reported in Fig. S2. As expected, the transform is characterized by a main frequency component at 13.5 MHz, and other minor frequency components. Furthermore, measurements of temperature and pH variations were performed for each experimental group to demonstrate that PEMF did not alter these parameters values. Results are shown in Fig. S3 and show that a temperature change of approximately −0.8 °C and a pH change of +0.3 were measured, which were comparable to those recorded during PEMF stimulation.

3.2. Carrier frequency screening on F11 cells

Immunofluorescence images of samples stimulated with PEMF at different carrier frequencies (F) are shown in Fig. 3a. The corresponding "Neurite length" distribution for neurite outgrowth quantification is shown in Fig. 3b for each experimental group. 13.5 MHz resulted in significantly longer neurites compared to the non-stimulated control ($p = 0.0113$), to 7.5 MHz ($p = 0.0025$), and 27 MHz ($p = 0.0282$). The "13.5 MHz" group did not show statistically significant differences compared to the "54 MHz" one ($p = 0.3511$); however, the average value of neurite length was slightly higher (44.10 *vs.* 28.70 μm). Cell viability was also tested. Results are reported in Fig. S4a. No statistically significant difference was detected between the different samples.

Based on these results, 13.5 MHz was chosen as the most appropriate F value for the following experimental sessions.

3.3. Pulse repetition frequency screening on F11 cells

Immunofluorescence images of samples stimulated with PEMF at different pulse repetition frequencies (PRF) are shown in Fig. 4a. The relative "Neurite length" distribution for neurites outgrowth quantification is shown in Fig. 4b for each experimental group. 20 Hz resulted in significantly longer neurites than the non-stimulated control ($p<0.0001$). The "20 Hz" group did not show statistically significant differences compared to the "5 Hz" group ($p = 0.8579$), the "50 Hz" group ($p = 0.6444$), and the "75 Hz" group ($p = 0.1046$). The average value of neurite length was slightly higher (52.67 μm for "20 Hz" *vs.* 45.64, 44.10, and 31.18 μm for "5 Hz", "50 Hz" and "75 Hz" respectively). Cell viability results are shown in Fig. S4b. No statistically significant difference was observed between the 20 Hz group and the non-stimulated control.

Based on these results, 20 Hz was chosen as the most appropriate PRF value for the following experimental sessions.

3.4. Duty cycle screening on F11 cells

Immunofluorescence images of samples stimulated with PEMF at different duty cycles (DC) are shown in Fig. 5a. The relative "Neurite length" distribution is shown in Fig. 5b for each experimental group. 10% resulted in significantly longer neurites than the non-stimulated

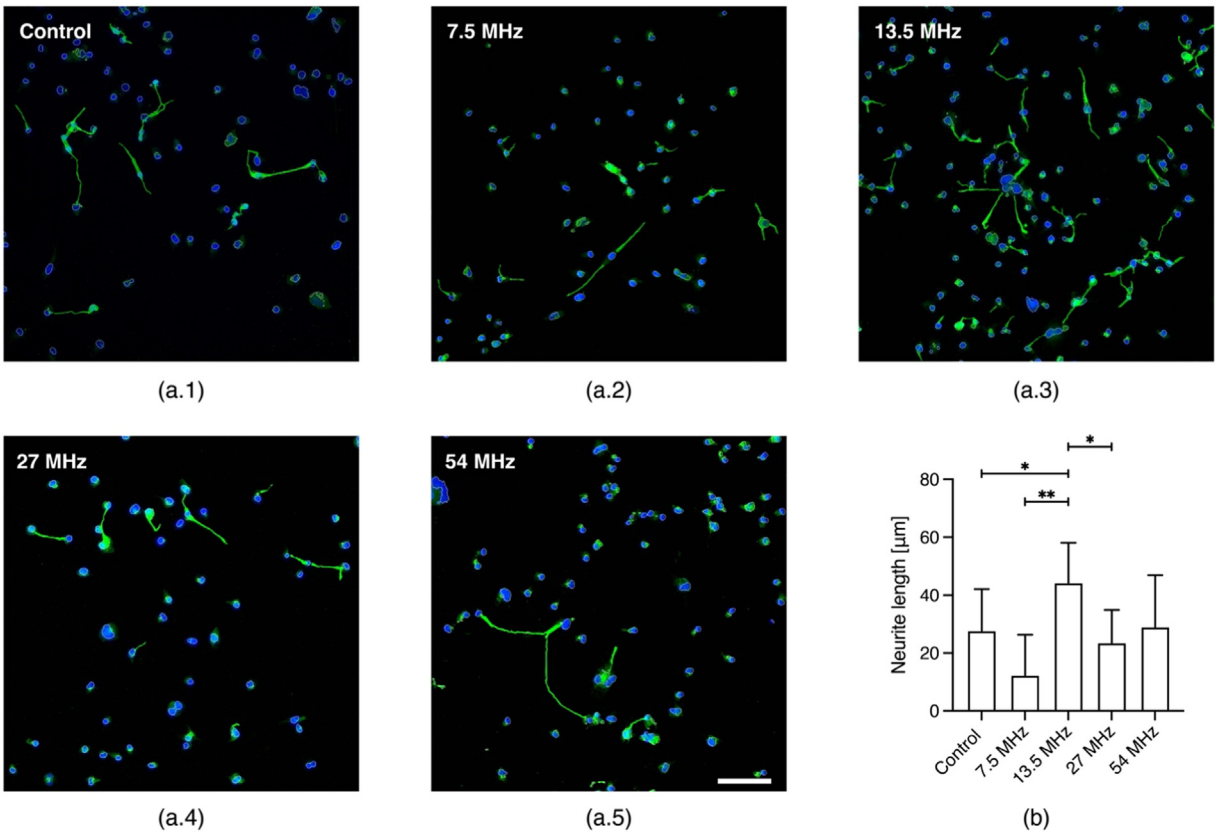

Fig. 3. Modulation of F11 neuron morphology in correspondence to different PEMF carrier frequencies. (a) Representative images of F11 cells, 24 h after the last exposure to PEMF stimulation, for four different carrier frequencies (7.5 MHz (a.2), 13.5 MHz (a.3), 27 MHz (a.4), and 54 MHz (a.5) and the non-stimulated case (Control (a.1)). The other parameters were kept constant: PRF = 50 Hz; DC = 10%; t = 3 h/d, for 3 days. In blue DAPI-stained nuclei are shown, whereas, in green, the β-III tubulin is shown. Scale bar = 100 μm. (b) Quantification of neuromorphometrics corresponding to the images shown in (a).

control (p<0.0001). The "10%" group did not show statistically significant differences compared to the "20%" group (p = 0.9477), the "30%" group (p = 0.2782), and the "40%" group (p = 0.1971); however, the average value of neurite length was slightly higher (52.67 μm for "10%" *vs.* 47.31, 37.11 and 35.62 μm for "20%", "30%" and "40%" respectively). Cell viability results are reported in Fig. S4c. No statistically significant difference was observed between the "Control," the "10%," and the "20%" groups.

Based on these results, the optimal PEMF stimulation conditions resulted in F = 13.5 MHz; PRF = 20 Hz; DC = 10%. These conditions were then applied to THP-1 cells.

3.5. Gene expression at the optimal PEMF conditions, on day 10

Fig. 6 shows the gene expression results for the analysis on day 10. In particular, regarding neuronal expression markers, NeuN showed an increase in gene expression on day 10 with respect to the unstimulated control at the same timepoint, whereas Tuj-1 showed an increase in gene expression on day 1, 3 and 10, with respect to the unstimulated control at the same timepoints. When considering transcription factors, Ngn1 did not show any statistical difference between stimulated and unstimulated groups, whereas NeuroD showed an increase in gene expression on day 10 with respect to the unstimulated samples. These results confirm the positive effects of the optimal PEMF conditions on neurogenesis.

3.6. THP-1 stimulation at the optimal PEMF conditions

Fig. S5 shows THP-1 cell images after staining with a LIVE/DEAD® Viability/Cytotoxicity Kit (Invitrogen). No significant differences in cell viability, morphology, and proliferation were observed.

The results concerning cytokine release are reported in Fig. 7, whereas gene expression is shown in Fig. 8. No significant differences were observed for all pro-inflammatory markers, between the "M0 + PEMF" and the "M0" groups, both in terms of cytokine release and gene expression. This confirmed that PEMF did not induce any inflammatory effect on cells. IL-8 cytokine release decreased in the "M0 + PEMF" group with respect to "M0". Furthermore, TNF-α and IL-8 release, as well as gene expression of IL-8 and IL-1β, decreased in the "M1 + PEMF" group compared to "M1", proving an anti-inflammatory effect induced by PEMF stimulation.

As expected, an anti-inflammatory effect was observed in the "M2" group with respect to the "M0" group (increased cytokine release of IL-10 and increased gene expression of IL-10 and CD206). IL-10 cytokine release increased in the "M0 + PEMF" group with respect to "M0", so demonstrating PEMF anti-inflammatory effect. The increase of IL-10 and CD206 gene expression supported this effect.

4. Discussion

To our knowledge, no prior state-of-the-art studies have investigated the *in vitro* effects of different PEMF stimulation parameters on F11 neuronal cells. First, we characterized the magnetic and electric field distribution in correspondence to biological samples (Fig. 2), also demonstrating that PEMF application did not induce any temperature and pH alteration in F11 cells. The complete characterization of the electromagnetic field in the stimulation area and the assessment of field homogeneity in the area occupied by the samples is an aspect not always addressed in similar works focused on PEMF stimulation [44]. Seo et al. [45], for example, promoted the regeneration of crush-injured rat nerves, by setting up an *ad hoc* PEMF stimulation system and applying

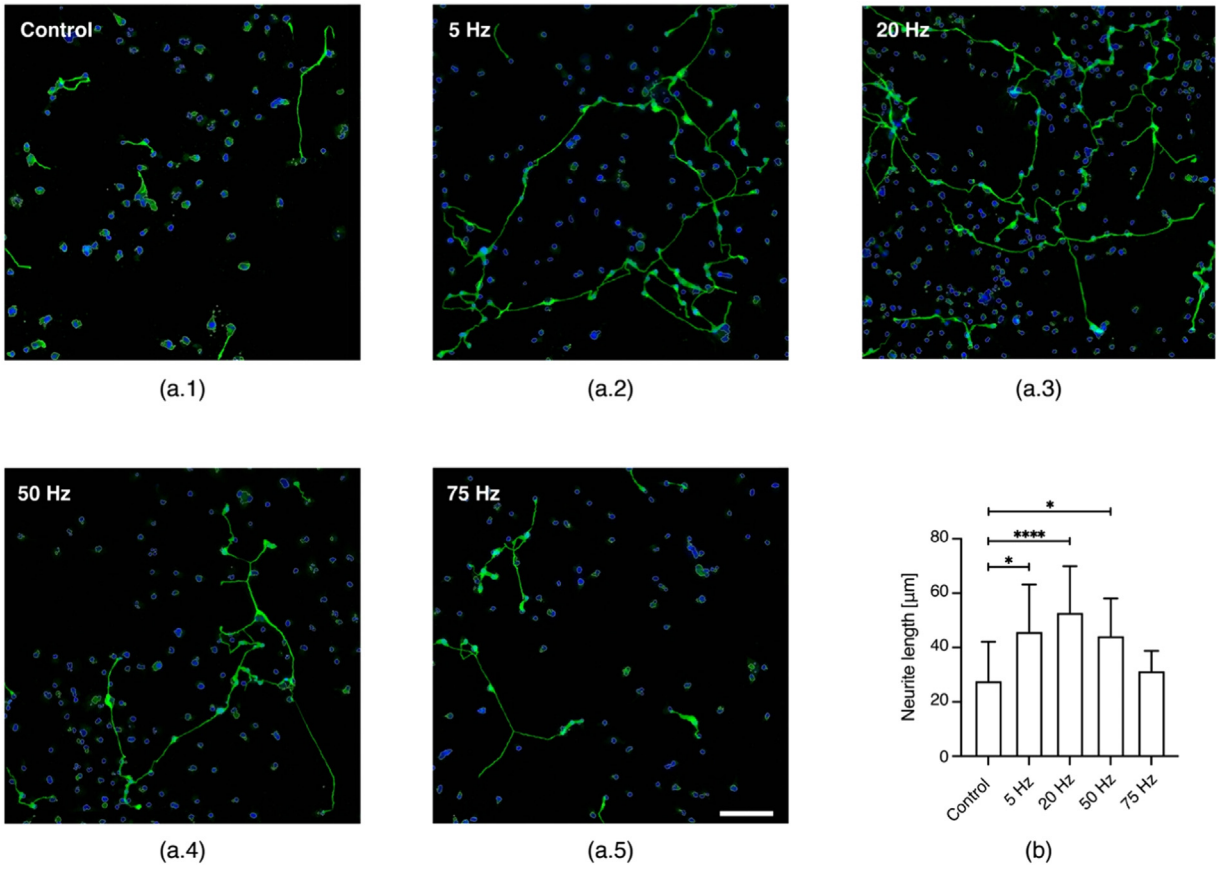

Fig. 4. Modulation of F11 neuron morphology in correspondence to different PEMF pulse repetition frequencies. (a) Representative images of F11 cells, 24 h after the last exposure to PEMF stimulation, for four different pulse repetition frequencies (5 Hz (a.2), 20 Hz (a.3), 50 Hz (a.4), and 75 Hz (a.5)) and the non-stimulated case (Control (a.1)). The other parameters were kept constant: F (Optimal) = 13.5 MHz; DC = 10%; t = 3 h/d for 3 days. In blue DAPI-stained nuclei are shown, whereas, in green, the β-III tubulin is shown. Scale bar = 100 μm. (b) Quantification of neuromorphometrics corresponding to the images shown in (a).

it to bone marrow-derived mesenchymal stem cells. Despite specifying some of their stimulation parameters, the homogeneity of the magnetic field and the induced electric field in the biological samples' area was not assessed, in this study. Yang et al. [46] applied PEMF to BV2 cells, a type of microglial cell, to assess possible anti-inflammatory protective effects against brain injury. Although the electromagnetic field output was measured through a Gaussmeter, its homogeneity in the entire center area of the Helmholtz coils, where the bottom of the cell culture plates was positioned, was not verified.

In the first experiment, we identified the optimal F value to trigger beneficial effects on neural cells. A significant increase in neurites outgrowth was registered at an F of 13.5 MHz (Fig. 3), with unaltered cell viability (Fig. S4). All the other tested F values (7.5, 27, and 54 MHz) did not show significant differences with respect to non-stimulated samples. The screening of different PEMF carrier frequencies has never been approached in the state-of-the-art, considering not only F11 cells but neural cells in general: Vincenzi et al. [16], for example, applied PEMF on PC12 (from rat pheochromocytoma) and SH-SY5Y (from human neuroblastoma), but did not specify the adopted F. Ma et al. [17] stimulated embryonic neural stem cells (from mice) by using PEMF, but, even in this case, the adopted value of central F was not reported.

When varying PRF, a dramatic increase in neurite outgrowth was observed in correspondence to a PRF of 20 Hz with respect to the control group (Fig. 4). The 5 Hz and 50 Hz groups also showed a significant increase with respect to the control group, but less evident. No difference was observed between the 75 Hz and the control group. These results suggested that, for that explored range, an increase in the energy transmitted (corresponding to a higher PRF) was useless for promoting neurite outgrowth. The optimal PRF range for neurite outgrowth was observed to be 5–50 Hz. Zhang et al. [15] observed longer neurites in PC12 cells at a PRF of 50 Hz, and an I between 0.19 and 1.37 mT, but no F was specified in this study.

Similarly, considering *in vivo* studies, Tavakoli et al. [38] were able to improve functional recovery and morphometric indices of rat sciatic nerve at an I of 0.3 mT (the same intensity used in this work) and a PRF of 2 Hz (t = 4 h/d for 1–5 days), a value that is quite close to the optimal PRF range found in our study. Also, Kanje et al. [36] also fostered rat sciatic nerve regeneration at an I of 0.3 mT and a PRF of 2 Hz (4 h/d for 1–4 days). None of these studies specified the adopted F, so limiting experimental repeatability.

An explanation of the efficacy of this PRF interval in inducing neural regenerative effects can be found in the electrical resonance phenomenon.

Electrical resonance occurs when a system (*e.g.*, a neural cell) oscillates with greater amplitude at a specific frequency [47]. It has been demonstrated that these oscillatory signals can influence connectivity between neurons, synaptic communication, and the rhythm of spike firing [48]. For mammalian neurons, the resonance frequency has been observed to range from 4 to 10 Hz [47]. The final optimal PRF range found in this study is reasonably consistent with the mammals' resonance frequency range. More studies would be needed to confirm this hypothesis and investigate the underlying mechanism, which is probably directly related to voltage-gated ion channels on the cell membrane [48]. In addition to that, in our study, a slight increase in viability, even if not statistically significant, was observed at a PRF of 20 Hz (Fig. S4b). It is known that neural regeneration is typically a highly energy-demanding process [49], so an enhanced metabolic activity is expected to benefit it.

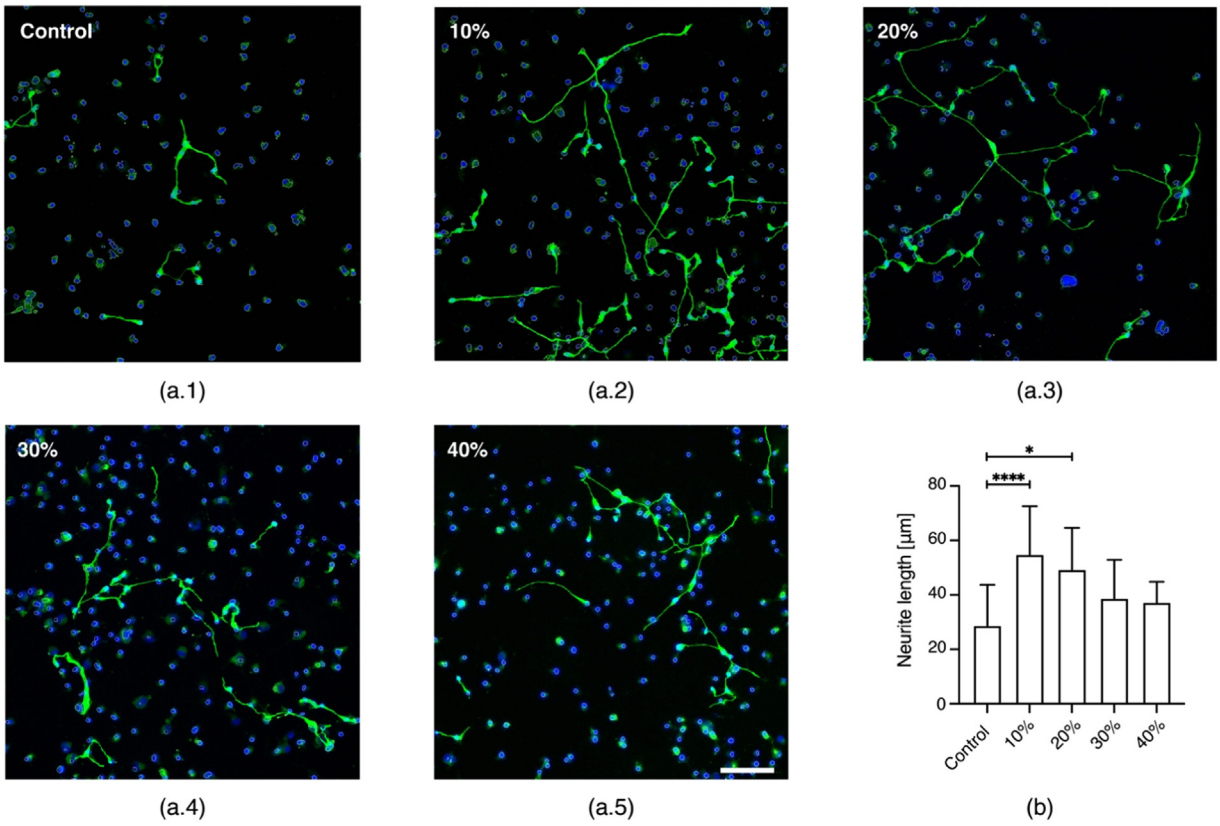

Fig. 5. Modulation of F11 neuron morphology in correspondence to different PEMF duty cycles. (a) Representative images of F11 cells, 24 h after the last exposure to PEMF stimulation, for four different duty cycles (10% (a.2), 20% (a.3), 30% (a.4), and 40% (a.5)) and the non-stimulated case (Control (a.1)). The other parameters were kept constant: F (Optimal) = 13.5 MHz; PRF (Optimal) = 20 Hz; t = 3 h/d for 3 days. In blue DAPI-stained nuclei are shown, whereas, in green, the β-III tubulin is shown. Scale bar = 100 μm. (b) Quantification of neuromorphometrics corresponding to the images shown in (a).

The last experimental session was devoted to the investigation of the optimal DC. No studies in the state-of-the-art have screened PEMF DC when stimulating neural cells. We found that a DC of 10% was the best value from a neuromorphometric and viability viewpoint. A dramatic decrease in neurite outgrowth was observed when increasing DC, going from 10% to 40%, proving that an increase in transmitted energy was partially harmful. A similar trend was also observed for viability. This behavior can be justified by comparing the stimulation rate to the neuron refractory period.

The refractory period is the interval following a neuron spike wherein the system cannot be excited again. It is a fundamental component of excitability, during which the neuron returns to its rest state, thus enabling repeatable spikes [50]. Generally, in a neuron, the refractory period lasts 1–2 ms [51]. By fixing a PRF of 20 Hz, the pulse period for DC screening tests was equal to 50 ms. When varying the DC between 10% and 40%, the pulse resulted in an interval between 5 and 20 ms, respectively, higher than the neuron physiological refractory period. It is known that, at low stimulation rates, the nerve cell response simply follows the stimulus. When the stimulation period equals the refractory period, firing occurs at its maximum. When stimulation rates are higher than the maximum action potential rate, the relationship between nerve cell response and stimulation rate turns unpredictable, especially if the stimulation alters the refractory period. Thus, the nerve cell response can increase and decrease as the pulse rate increases [52]. This could explain what was observed in our study: DC could have altered the polarization of nerve membrane, affecting signaling in neurons and reducing neurite outgrowth and cell viability. However, future analysis would be needed to verify such a hypothesis.

Once the optimal stimulation condition for promoting regenerative effects on F11 cells was identified (F = 13.5 MHz, PRF = 20 Hz, DC = 10%), we verified the effects of this condition on long-term gene expression of F11 cells. A time-point of 10 days, after PEMF stimulation, was considered as nerve repair is a long-term process and this could have provided a more comprehensive understanding of the effects of PEMF stimulation over time. In particular, we focused on neuronal expression markers NeuN and Tuj-1 and on transcription factors Ngn1 and NeuroD, which are known to be closely related to neurogenesis [29,30]. The most positive and beneficial results are represented by Tuj-1 gene expression increase, already boosted 24 h after PEMF stimulation with respect to control and remaining statistically unaltered at day 3 and day 10; as well as NeuroD and NeuN gene expression increase, with a significant boost 10 days after PEMF stimulation. Von Bohlen and Halbach [53] schematized the neurogenesis mechanism into five consecutive stages, with main relative markers: proliferation (nestin), differentiation (nestin, Pax6), migration (NeuroD, DCX, PSA-NCAM), axonal and dendritic targeting (PSA-NCAM, DCX, TUC-4, Calretinin), and finally synaptic integration (NeuN, Tuj-1; Calbindin). More specifically, if on one hand Tuj-1 is expressed mostly by neuronal progenitor cells and immature granule cells, NeuN is mainly expressed by mature granule cells. The achieved results not only confirmed and respected the temporal development of neural differentiation (as NeuN gene expression increased lately with respect to that of Tuj-1) but also proved that this differentiation was significantly promoted and accelerated 10 days after PEMF stimulation.

The same optimal stimulation condition was also considered to demonstrate whether it could modulate inflammatory conditions on THP-1 cells. Understanding their effects on immune cells is paramount, given the crucial role of inflammation in nerve injury processes, given a future preclinical and clinical application of these parameters for neural regeneration. [6]. Indeed, such condition induced anti-inflammatory

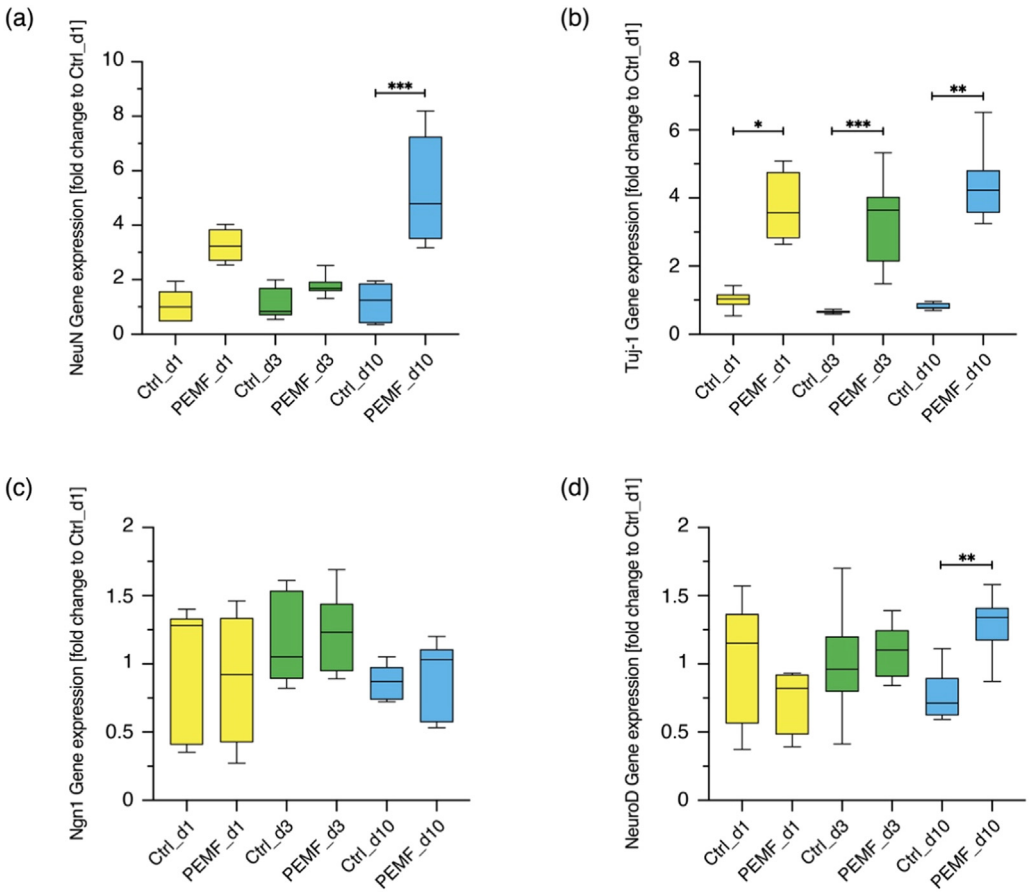

Fig. 6. Gene expression of neuronal expression markers NeuN (a) and Tuj-1 (b), and of transcription factors Ngn1 (c) and NeuroD (d) (only the optimal stimulation condition was considered for the "PEMF" group, namely: F = 13.5 MHz; PRF = 20 Hz; DC = 10%).

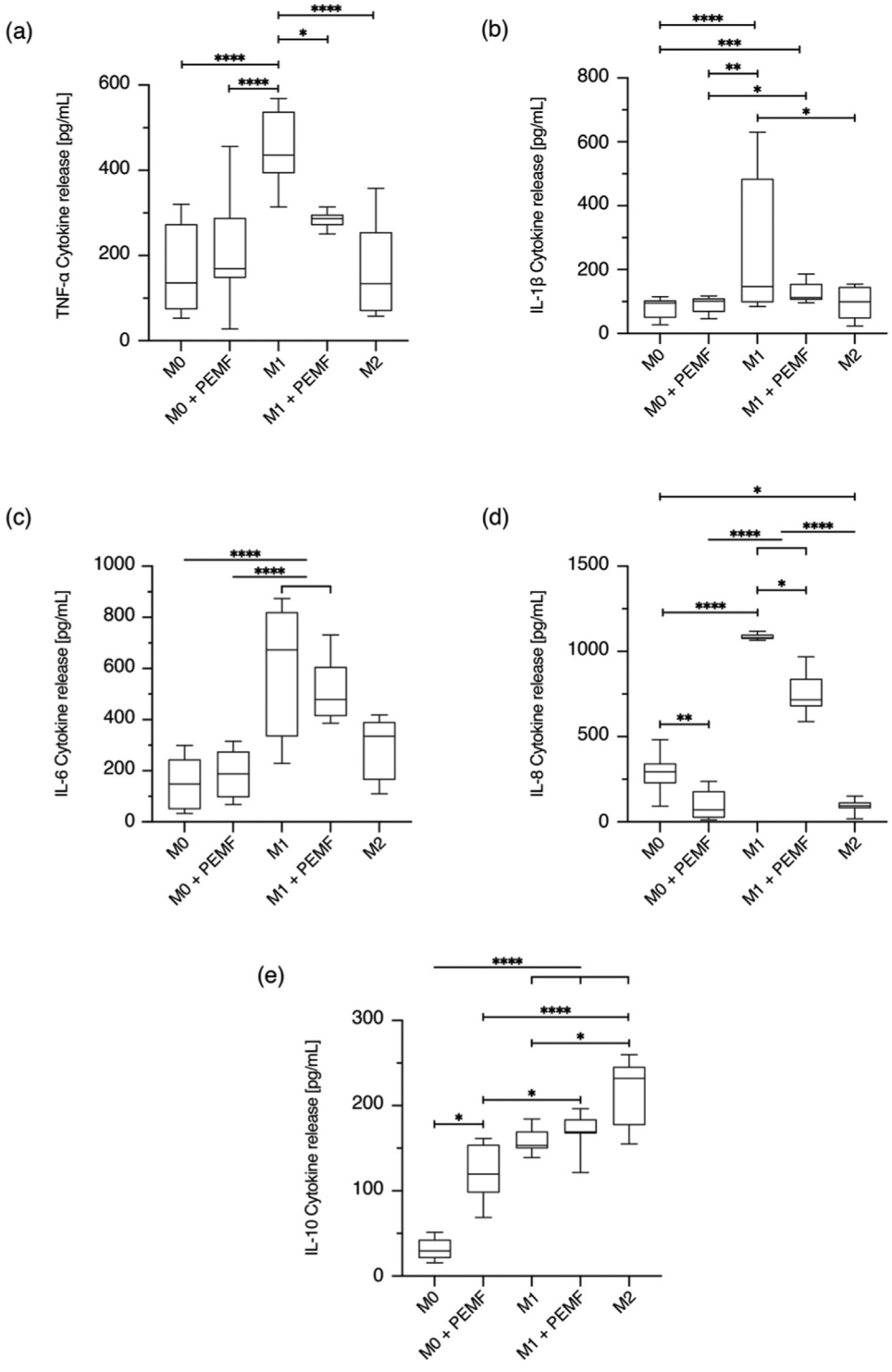

Fig. 7. Pro-inflammatory markers (TNF-α (a), IL-1β (b), IL-6 (c), IL-8 (d)) and anti-inflammatory marker IL-10 (e) cytokine release, for THP-1 cells, for all experimental groups ("M0 + PEMF" and "M1 + PEMF" were stimulated at the optimal condition, namely: F = 13.5 MHz, PRF = 20 Hz, DC = 10%). .

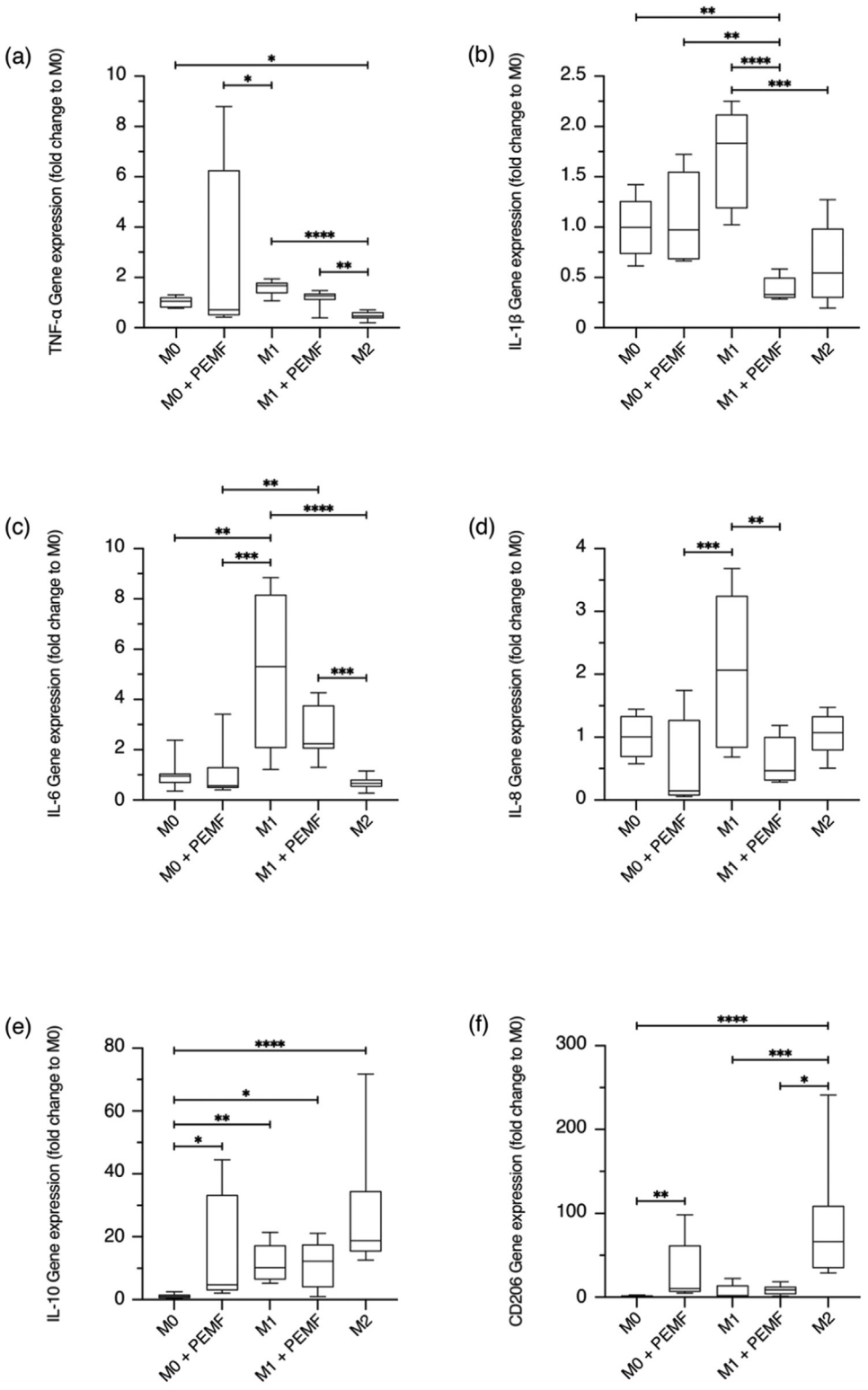

Fig. 8. Pro-inflammatory markers (TNF-α (a), IL-1β (b), IL-6 (c) and IL-8 (d)) and anti-inflammatory markers (IL-10 (e) and CD206 (f)) gene expression, for THP-1 cells, for all experimental groups ("M0 + PEMF" and "M1 + PEMF" were stimulated at the optimal condition, namely: F = 13.5 MHz, PRF = 20 Hz, DC = 10%). Genes were expressed as fold changes with respect to "M0".

effects in THP-1 cells (Figs. 7 and 8). Ross *et al.* (2019) [54] examined the effects of PEMF on immune cells, finding that the following condition: I = 0.04 mT, PRF = 5.1 Hz, t = 5 min (for one day) was able to decrease pro-inflammatory cytokines secretion (IL-1β, IL-6, and TNF-α) and stabilize anti-inflammatory cytokines secretion (IL-10). Patruno et al. (2020) [55] observed that PEMF stimulation at the following condition: I = 1 mT, PRF = 50 Hz, t = 6 h (for one day) had protective effects on LPS-treated THP-1 cells, in terms of activation of anti-inflammatory intracellular pathways (Nrf2 and HO-1). The outcomes of these studies are not entirely comparable to the ones shown in this work since the stimulation conditions were different. However, they confirm that different PEMF stimulation regimes can produce anti-inflammatory effects.

5. Conclusions

In this work, different PEMF stimulation parameters (carrier frequency - F, pulsed repetition frequency - PRF, and duty cycle - DC) were systematically screened to trigger beneficial (pro-regenerative) effects on F11 neural cells *in vitro*. The following parameter values: F = 13.5 MHz, PRF = 20 Hz, DC = 10% (with an I of 0.3 mT and a t of three h/d for three days) were identified as the optimal ones for enabling neural regeneration in terms of neurite outgrowth. This was also confirmed by gene expression results, which suggested a neurogenesis promotion and acceleration 10 days after PEMF stimulation.

Furthermore, such an optimal stimulation condition was also applied to THP-1 cells, differentiated into M1 and M2 phenotypes. PEMF did not induce any differentiation towards M1 phenotype, decreased cytokine level and gene expression of pro-inflammatory markers in M1-differentiated macrophages, and increased gene expression of anti-inflammatory markers in M0 macrophages. These results pave the way for future studies that may further investigate the underlying mechanisms of cell responses and for a translation of this technology, which can be applied directly to patients, thanks to the already proven safety of PEMF stimulation regimes.

Declaration of Competing Interest

The authors declare that they have no known competing financial interests or personal relationships that could have appeared to influence the work reported in this paper. The involvement of BAC Technology s.r.l. in the project did not influence the result collection, analysis, and interpretation.

CRediT authorship contribution statement

Francesco Fontana: Validation, Formal analysis, Investigation, Data curation, Writing – original draft, Writing – review & editing, Visualization. **Andrea Cafarelli:** Methodology, Data curation, Writing – review & editing, Visualization, Supervision, Project administration. **Francesco Iacoponi:** Validation, Formal analysis, Data curation, Writing – review & editing, Visualization. **Soria Gasparini:** Formal analysis, Data curation, Writing – review & editing, Visualization. **Tiziano Pratellesi:** Resources, Writing – review & editing. **Abigail N. Koppes:** Conceptualization, Methodology, Resources, Writing – review & editing, Supervision, Project administration, Funding acquisition. **Leonardo Ricotti:** Conceptualization, Methodology, Resources, Writing – review & editing, Supervision, Project administration, Funding acquisition.

Acknowledgments

This work has received funding from the “UltraHeal” Project, in collaboration with BAC Technology s.r.l. (Florence, Italy). The authors thank the Department of Chemical Engineering at Northeastern University, Boston, MA 02115, USA. The authors declare that they have no known competing financial interests or personal relationships that could have appeared to influence the work reported in this paper. The involvement of BAC Technology s.r.l. did not influence the result collection, analysis, and interpretation.

Supplementary materials

Supplementary material associated with this article can be found, in the online version, at doi:10.1016/j.engreg.2023.11.003.

References

[1] N.Y. Li, et al., Epidemiology of peripheral nerve injuries in sports, exercise, and recreation in the united, Phys. Sportsmed. 00 (00) (2020) 1–8.
[2] M.L. Wang, et al., Peripheral nerve injury, scarring, and recovery, Connect. Tissue Res. 60 (1) (2019) 3–9.
[3] C.R. Carvalho, J.M. Oliveira, R.L. Reis, Modern trends for peripheral nerve repair and regeneration: beyond the hollow nerve guidance conduit, Front. Bioeng. Biotechnol. 7 (November) (2019) 1–30.
[4] S.A. Nesbit, et al., Non-pharmacologic treatments for symptoms of diabetic peripheral neuropathy: a systematic review, Curr. Med. Res. Opin. 35 (1) (2019) 15–25.
[5] G. Orlando, Regenerative Medicine Applications in Organ Transplantation, Academic Press, 2014.
[6] E. Ydens, et al., Acute injury in the peripheral nervous system triggers an alternative macrophage response, J. Neuroinflamm. 9 (2012) 1–17.
[7] C. Salgado, F. Vilson, N.R. Miller, S.L. Bernstein, Cellular inflammation in nonarteritic anterior ischemic optic neuropathy and its primate model, Arch. Ophthalmol. 129 (12) (2011) 1583–1591.
[8] F. Fregnan, L. Muratori, A.R. Simões, M.G. Giacobini-Robecchi, S. Raimondo, Role of inflammatory cytokines in peripheral nerve injury, Neural Regen. Res. 7 (29) (2012) 2259–2266.
[9] B. Wade, A review of pulsed electromagnetic field (PEMF) mechanisms at a cellular level: a rationale for clinical use, Am. J. Heal. Res. 1 (3) (2013) 51.
[10] K. Hug, M. Röösli, Therapeutic effects of whole-body devices applying pulsed electromagnetic fields (PEMF): a systematic literature review, Bioelectromagnetics 33 (2) (2012) 95–105.
[11] J.S. Gaynor, S. Hagberg, B.T. Gurfein, Veterinary applications of pulsed electromagnetic field therapy, Res. Vet. Sci. 119 (May) (2018) 1–8.
[12] R. Lekhraj, D.E. Cynamon, S.E. Deluca, E.S. Taub, A.A. Pilla, D. Casper, Pulsed electromagnetic fields potentiate neurite outgrowth in the dopaminergic MN9D cell line, J. Neurosci. Res. 92 (6) (2014) 761–771.
[13] L. Cristiano, T. Pratellesi, Mechanisms of action and effects of pulsed electromagnetic fields (PEMF) in medicine, J. Med. Res. Surg. 1 (6) (2020) 1–4.
[14] R. Dennis, PEMF: a survey of clinical and individual uses and perceptions, J. Sci. Med. 3 (2) (2021) 1–46.
[15] Y. Zhang, J. Ding, W. Duan, A study of the effects of flux density and frequency of pulsed electromagnetic field on neurite outgrowth in PC12 cells, J. Biol. Phys. 32 (1) (2006) 1–9.
[16] F. Vincenzi, et al., Pulsed electromagnetic field exposure reduces hypoxia and inflammation damage in neuron-like and microglial cells, J. Cell. Physiol. 232 (5) (2017) 1200–1208.
[17] Q. Ma, et al., Extremely low-frequency electromagnetic fields promote *in vitro* neuronal differentiation and neurite outgrowth of embryonic neural stem cells via up-regulating TRPC1, PLoS ONE 11 (3) (2016) 1–21.
[18] Y. Li, et al., Pulsed electromagnetic field enhances brain-derived neurotrophic factor expression through L-type voltage-gated calcium channel- and Erk-dependent signaling pathways in neonatal rat dorsal root ganglion neurons, Neurochem. Int. 75 (2014) 96–104.
[19] C.L. Ross, B.S. Harrison, Effect of pulsed electromagnetic field on inflammatory pathway markers in RAW 264.7 murine macrophages, J. Inflamm. Res. 6 (1) (2013) 45–51.
[20] S. Groiss, R. Lammegger, Anti-oxidative and immune regulatory responses of THP-1 and PBMC to Pulsed EMF are field-strength dependent, Int. J. Environ. Res. Public Health 18 (18) (2021) 9519.
[21] H. Hu, et al., Promising application of Pulsed Electromagnetic Fields (PEMFs) in musculoskeletal disorders, Biomed. Pharmacother. 131 (2020) 110767.
[22] A.E. Mocanu-Dobranici, M. Costache, S. Dinescu, Insights into the molecular mechanisms regulating cell behavior in response to magnetic materials and magnetic stimulation in stem cell (neurogenic) differentiation, Int. J. Mol. Sci. 24 (3) (2023).
[23] F.J. Stam, et al., Identification of candidate transcriptional modulators involved in successful regeneration after nerve injury, Eur. J. Neurosci. 25 (12) (2007) 3629–3637.
[24] M.R. Tannemaat, et al., Human neuroma contains increased levels of semaphorin 3A, which surrounds nerve fibers and reduces neurite extension in vitro, J. Neurosci. 27 (52) (2007) 14260–14264.
[25] K. Yin, G.J. Baillie, I. Vetter, Neuronal cell lines as model dorsal root ganglion neurons: a transcriptomic comparison, Mol. Pain 12 (2016) 1–17.
[26] J. Prucha, J. Krusek, I. Dittert, V. Sinica, A. Kadkova, V. Vlachova, Acute exposure to high-induction electromagnetic field affects activity of model peripheral sensory neurons, J. Cell. Mol. Med. 22 (2) (2018) 1355–1362.
[27] N.Z. Borgesius, et al., βCaMKII plays a nonenzymatic role in hippocampal synaptic plasticity and learning by targeting α;CaMKII to synapses, J. Neurosci. 31 (28) (2011) 10141–10148.
[28] P. Wieringa, I. Tonazzini, S. Micera, M. Cecchini, Nanotopography induced contact guidance of the F11 cell line during neuronal differentiation: a neuronal model cell line for tissue scaffold development, Nanotechnology 23 (27) (2012).

[29] G. Longfei, et al., Direct generation of human neuronal cells from adult astrocytes by small molecules, Stem Cell Rep. 8 (2017) 538–547.
[30] S. Seo, J.W. Lim, D. Yellajoshyula, L.W. Chang, K.L. Kroll, Neurogenin and NeuroD direct transcriptional targets and their regulatory enhancers, EMBO J. 26 (24) (2007) 5093–5108.
[31] C. Zhan, C. Ma, H. Yuan, B. Cao, J. Zhu, Macrophage-derived microvesicles promote proliferation and migration of Schwann cell on peripheral nerve repair, Biochem. Biophys. Res. Commun. 468 (1–2) (2015) 343–348.
[32] T.C. Huang, H.L. Wu, S.H. Chen, Y.T. Wang, C.C. Wu, Thrombomodulin facilitates peripheral nerve regeneration through regulating M1/M2 switching, J. Neuroinflammation 17 (1) (2020) 1–14.
[33] V. Pastori, A. D'Aloia, S. Blasa, M. Lecchi, Serum-deprived differentiated neuroblastoma F-11 cells express functional dorsal root ganglion neuron properties, PeerJ 2019 (10) (2019) 1–20.
[34] F. Fontana, F. Iacoponi, F. Orlando, T. Pratellesi, A. Cafarelli, L. Ricotti, Low-intensity pulsed ultrasound increases neurotrophic factors secretion and suppresses inflammation in *in vitro* models of peripheral neuropathies, J. Neur. Eng. 20 (2) (2023) 026033.
[35] G.C. Goats, Pulsed electromagnetic (short-wave) energy therapy, Br. J. Sports Med. 23 (4) (1989) 213–216.
[36] M. Kanje, A. Rusovan, B. Sisken, G. Lundborg, Pretreatment of rats with pulsed electromagnetic fields enhances regeneration of the sciatic nerve, Bioelectromagnetics 14 (4) (1993) 353–359.
[37] J.L. Walker, R. Kryscio, J. Smith, A. Pilla, B.F. Sisken, Electromagnetic field treatment of nerve crush injury in a rat model: effect of signal configuration on functional recovery, Bioelectromagnetics 28 (4) (2007) 256–263.
[38] P. Tavakoli, Effects of pulsed electromagnetic fields on peripheral nerve regeneration using allografts in sciatic nerve: an animal model study, Biomed. J. Sci. Tech. Res. 1 (6) (2017) 1667–1673.
[39] R. Mohammadi, D. Faraji, H. Alemi, A. Mokarizadeh, Pulsed electromagnetic fields accelerate functional recovery of transected sciatic nerve bridged by chitosan conduit: an animal model study, Int. J. Surg. 12 (12) (2014) 1278–1285.
[40] D. Ventre, M. Puzan, E. Ashbolt, A. Koppes, Enhanced total neurite outgrowth and secondary branching in dorsal root ganglion neurons elicited by low intensity pulsed ultrasound, J. Neural Eng. 15 (4) (2018).
[41] T. Torregrosa, et al., Cryopreservation and functional analysis of cardiac autonomic neurons, J. Neurosci. Method. 341 (September 2019) (2020) 108724.
[42] D. Diaz, J.R. Soucy, A. Lee, R.A. Koppes, A.N. Koppes, Light irradiation of peripheral nerve cells : wavelength impacts primary sensory neuron outgrowth *in vitro*, J. Photochem. Photobiol. B Biol. 215 (May 2020) (2021) 112105.
[43] A.N. Koppes, A.N. Seggio, D.M. Thompson, Neurite outgrowth is significantly increased by the simultaneous presentation of Schwann cells and moderate exogenous electric fields, J. Neur. Eng. (2011).
[44] S. Grehl, D. Martina, C. Goyenvalle, Z. Deng, *In vitro* magnetic stimulation : a simple stimulation device to deliver defined low intensity electromagnetic fields, Front. Neur. Circuit. 10 (2016) 85.
[45] N.R. Seo, et al., Low-frequency pulsed electromagnetic field pretreated bone marrow-derived mesenchymal stem cells promote the regeneration of crush-injured rat mental nerve, Neur. Regen. Res. 13 (1) (2018) 145–153.
[46] Y. Yang, et al., Pulsed Electromagnetic Field Protects Against Brain Injury After Intracerebral Hemorrhage: involvement of Anti-Inflammatory Processes and Hematoma Clearance via CD36, J. Mol. Neurosci. 72 (10) (2022) 2150–2161.
[47] E. Stark, H.G. Rotstein, Neuronal resonance can be generated independently at distinct levels of organization, bioRxiv (2020) 1–34.
[48] L. Ge, X.D. Liu, Electrical resonance with voltage-gated ion channels: perspectives from biophysical mechanisms and neural electrophysiology, Acta Pharmacol. Sin. 37 (1) (2016) 67–74.
[49] J.R. Valcourt, J.M.S. Lemons, E.M. Haley, M. Kojima, O.O. Demuren, H.A. Coller, Metabolic adaptations to quiescence, Cell Cycle 11 (9) (2012) 1680–1696.
[50] H.T. Peng, et al., Temporal information processing with an integrated laser neuron, IEEE J. Sel. Top. Quant. Electron. 26 (1) (2020).
[51] Q. Gan, Y.U. Wei, Neural modeling with dynamically adjustable threshold and refractory period, Biosystems 27 (3) (1992) 137–144.
[52] V. Krauthamer, T. Crosheck, Effects of high-rate electrical stimulation upon firing in modelled and real neurons, Med. Biol. Eng. Comput. 40 (3) (2002) 360–366.
[53] O. Von Bohlen Und Halbach, Immunohistological markers for staging neurogenesis in adult hippocampus, Cell Tiss. Res. 329 (3) (2007) 409–420.
[54] C.L. Ross, Y. Zhou, C.E. Mccall, S. Soker, T.L. Criswell, The use of pulsed electromagnetic field to modulate inflammation and improve tissue regeneration : a review, Bioelectricity 1 (4) (2019) 247–259.
[55] A. Patruno, et al., Short ELF-EMF exposure targets SIRT1 /Nrf2 / HO-1 signaling in THP-1 cells, Int. J. Mol. Sci. 21 (19) (2020) 7284.